PHYSICAL REVIEW B **72**, 121304(R) (2005)

Edge magnetoplasmons in quantum Hall line junction systems

Wei-Cheng Lee,* N. A. Sinitsyn, Emiliano Papa, and A. H. MacDonald†
Department of Physics, The University of Texas at Austin, Austin, Texas 78712, USA
(Received 8 July 2005; published 15 September 2005)

A quantum Hall line junction system consists of a one-dimensional Luttinger liquid (LL) and two chiral channels that allow density waves incident upon and reflected by the LL to be measured separately. We demonstrate that interactions in a quantum Hall line junction system can be probed by studying edge magnetoplasmon absorption spectra and their polarization dependences. Strong interactions in the junction lead to collective modes that are isolated in either Luttinger liquid or contact subsystems.

DOI: 10.1103/PhysRevB.72.121304 PACS number(s): 73.43.Fj, 73.43.Lp

A quantum Hall line junction[1–3] (QHLJ) enables the realization of one-dimensional electron systems with widely tunable properties. A line junction is generated by creating a narrow barrier that divides a two-dimensional electron system on a quantum Hall plateau into separate subsystems as illustrated in Fig. 1. Chiral quantum Hall edge channels[4–6] flow in opposite directions on opposite sides of the barrier and constitute a nonchiral one-dimensional electron gas. An attractive feature of QHLJ systems is the physical separation of incident and reflected states at the ends of the nonchiral barrier region, a benefit provided by the chiral quantum Hall edge states. This feature plays a role, for example, in proposed electron teleportation effects[7] on quantum Hall edges.

The narrow barriers that define QHLJs can be realized by cleaved edge overgrowth,[8] corner overgrowth,[9] or by the deposition of narrow metallic gates.[10–12] Experimental studies of various QHLJ systems, and some of the theoretical analyses[13–16] that they have motivated, have made it clear that interactions between electrons on opposite sides of the barrier can play an essential role in their physics. An important difficulty that arises in interpreting the transport properties of QHLJ systems is uncertainty about the strength and sometimes even the sign of these interactions, which can be difficult to estimate because of subtleties[17] in understanding their relationships to underlying Coulombic interactions, and, in some systems, because of edge reconstructions[18] or the role played by nearby metallic gates.[19] In this paper we propose that measurement of edge magnetoplasmon[20] properties in QHLJ systems can provide the required information experimentally. To illustrate the potential of this approach, we derive analytic expressions for the edge magnetoplasmon spectrum of a simple QHLJ model and present numerical results of power absorption spectrum. The relevance of the simple model to a more realistic model is also discussed. We find that as interactions across the barrier strengthen, the independent magnetoplasmon excitations of the separated quantum Hall regions evolve into two quite distinct modes, a plasmon excitation localized along the barrier and a chiral magnetoplasmon mode that extends along the entire boundary of the compound system. This change in character of the excitation spectrum, and accompanying changes in the strength of resonant absorption of electromagnetic (EM) radiation polarized either along or perpendicular to the barrier, can be used to reliably estimate the strength and sign of interactions across the barrier.

Edge Magnetoplasmon Excitations of the QHLJ Model. We concentrate in this paper on the case of $\nu=1$ quantum Hall states for which the low-energy edge physics can, in the absence of reconstructions[18] be entirely[4] described in terms of the edge charge densities $\rho_L(x)$ and $\rho_R(x)$, of the left and right quantum Hall edges. The QHLJ model that we use to obtain a qualitative understanding of the magnetoplasmon spectrum includes interactions between left and right subsystems only in the barrier region,

$$H = H_0 + H_i,$$

$$H_0 = \pi\hbar v_f \int_0^P dx[\rho_L(x)\rho_L(x) + \rho_R(x)\rho_R(x)],$$

$$H_i = 2\pi\hbar v_f g \int_0^P dx F(x)\rho_L(x)\rho_R(x), \tag{1}$$

where H_0 neglects interactions between separate edges, v_f is the chiral edge mode velocity of an isolated subsystem, and H_i describes interactions across the barrier. The parameter g is the ratio of interactions across the barrier to self-interactions on an isolated edge and P is the total perimeter of the individual quantum Hall regions. We measure distances along the edges using the coordinate system explained in Fig. 1 so that $F(x) \equiv \theta(x) - \theta(x-W)$ where W is the width

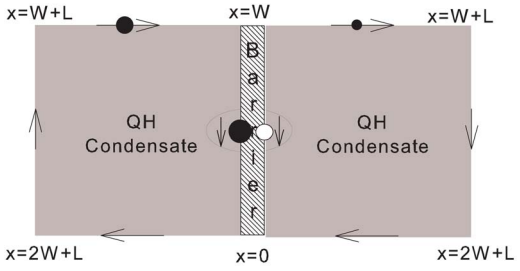

FIG. 1. (Color online) Cartoon of a QH line junction. The circles and arrows illustrate, for the case of repulsive interactions of moderate strength, the evolution of a unit charge incident on the top of the Lutinger liquid discussed in the text. The total perimeter of each QH region is $P=2W+2L$ and, in the coordinate system we use, the barrier region is the interval $[0,W]$.

of the Hall bar. For $\nu=1$ this model can be quantized by imposing the commutation relations,[4]

$$[\rho_L(x),\rho_L(x')]=\left(\frac{i}{2\pi}\right)\partial_x\delta(x-x'),$$

$$[\rho_R(x),\rho_R(x')]=-\left(\frac{i}{2\pi}\right)\partial_x\delta(x-x'),$$

$$[\rho_L(x),\rho_R(x')]=0. \tag{2}$$

It follows that the equations of motion for ρ_L and ρ_R are

$$-\partial_t\rho_L(x,t)=-v_f\partial_x[\rho_L(x,t)+gF(x)\rho_R(x,t)],$$

$$-\partial_t\rho_R(x,t)=v_f\partial_x[\rho_R(x,t)+gF(x)\rho_L(x,t)]. \tag{3}$$

The right-hand sides of Eqs. (3) provide expressions for the current densities on left and right edges, $j_L(x)=-v_f[\rho_L(x,t)+gF(x)\rho_R(x,t)]$ and $j_R(x)=v_f[\rho_R(x,t)+gF(x)\rho_L(x,t)]$. Equations (3) are readily solved for fixed g, and solutions in the $g=0$ and $g\neq 0$ regions can be matched by requiring that the current densities be continuous.[21,22] The general solution is most conveniently expressed in terms of fields $\phi_{L,R}(x)$, related to the charge densities by $\rho_{L,R}(x,t)=\pm\partial_x\phi_{L,R}(x,t)/(2\pi)$. The matching condition that $j_{L,R}$ should be continuous is equivalent to the condition that normal mode $\phi_{L,R}$ solutions at each frequency ω should be continuous. The general form of a normal mode with frequency ω in the barrier region is

$$\phi_L(x)=A\exp(iqx)+B\exp(-iqx),$$

$$\phi_R(x)=A\frac{\sqrt{1-g^2}-1}{g}\exp(iqx)-B\frac{\sqrt{1-g^2}+1}{g}\exp(-iqx), \tag{4}$$

where $q=\omega/(v_f\sqrt{1-g^2})$.

The evolution of a unit impulse charge traveling along a chiral edge can be understood on the basis of Eq. (4), charge conservation along both edges, the chirality of the outer edges, and the reduced wave velocity along the barrier. A unit impulse charge approaching the barrier from the left along the top of the Hall bar must launch an impulse that travels down along the barrier in order to conserve charge along the left edge. Since this density wave travels at a slower velocity v_I, it must have left-edge charge density that is larger by the factor of $v_f/v_I=1/\sqrt{1-g^2}$. The equations of motion in the barrier region imply that the ratio of right-side charge to left-side charge for a downward traveling barrier wave is $(\sqrt{1-g^2}-1)/g$ so that a downward traveling charge is also induced on the right-hand side of the barrier. To conserve right-edge charge, a chiral edge wave traveling at the higher velocity with charge $(1-\sqrt{1-g^2})/g$ must also be launched on the upper right. This part of the edge density wave may be regarded as the chiral lead component that has been reflected by the barrier. A QHLJ system, however, is spatially separated from the incoming wave. The total current traveling down the barrier approaches 0 for $g\to 1$ and $2v_f$ for $g\to -1$. These conclusions argued for here on the basis of charge conservation and equations of motion also follow from the matching conditions discussed previously. Each of the waves launched by the original impulse will bifurcate when it intersects with an edge-barrier boundary.

To determine the normal mode frequencies we integrate ϕ_L and ϕ_R around their respective edges and apply the single-valuedness condition:

$$\begin{pmatrix}\phi_L(P)\\ \phi_R(P)\end{pmatrix}=\begin{pmatrix}U_{LL} & U_{LR}\\ U_{RL} & U_{RR}\end{pmatrix}\begin{pmatrix}\phi_L(0)\\ \phi_R(0)\end{pmatrix}=\begin{pmatrix}\phi_L(0)\\ \phi_R(0)\end{pmatrix}. \tag{5}$$

Normal modes occur when the determinant of $U_{I,J}-\delta_{I,J}$ vanishes. In Eq. (5), $U^*_{RR}=U_{LL}$, $U^*_{LR}=U_{RL}$,

$$U_{LL}=e^{iq_0P'}\left(\cos(q_IW)+\tfrac{i}{\sqrt{1-g^2}}\sin(q_IW)\right),$$

$$U_{LR}=i\tfrac{g}{\sqrt{1-g^2}}e^{iq_0P'}\sin(q_IW), \tag{6}$$

$q_0=\omega/v_f$ and $q_I=q_0/\sqrt{1-g^2}$ are the local wave vectors in chiral and barrier regions, $P'=2L+W$ is the part of the perimeter of a quantum Hall region that is not along the barrier and $P'+W=P$ is the total perimeter. We have, for illustrative purposes, assumed that the two quantum Hall regions are identical. The collective mode frequencies solve

$$\cos(q_0P')\cos(q_IW)-\frac{\sin(q_0P')\sin(q_IW)}{\sqrt{1-g^2}}=1. \tag{7}$$

Weak Interaction Limit. In the absence of interactions across the barrier ($q_I=q_0, g=0$), Eq. (7) implies that the magnetoplasmon reference frequencies are given by $f_n=\omega_n/2\pi=nv_f/P$. The period of the fundamental edge magnetoplasmon mode is just the transit time for an edge wave to move entirely around an individual incompressible region, implying that two independent modes occur at each frequency. Since typical edge magnetoplasmon velocities[20] are $\sim 10^6$ m/s, frequencies are in the gigahertz range for samples with perimeters in the millimeter range. Weak interactions shift and split the independent incompressible region eigenmodes. From Eq. (7) we find that for small g

$$f_n=v_f/P[n\pm g\sin(2\pi nL/P)/2\pi+\cdots]. \tag{8}$$

If the sample geometry is known, g can be extracted from a measurement of the mode splitting.

Strong Interaction Limit. For $|g|$ that can be close to 1, the instability limit, the collective modes are determined by the conditions $\sin(q_0P')=0$ and $\sin(q_IW)=0$, leading to two sets of equally spaced modes with distinct fundamental frequencies at $f_0=v_f/2P'$ and $f_I=v_I/2W$. Apparently the edge magnetoplasmon modes in the strong interaction limit consist of independent modes localized along the barrier and along the chiral leads. The periods $2P'/v_f$ and $2W/v_I$, respectively, correspond to the transit times for a wave traveling around the combined outer chiral edge at velocity v_f and a wave traveling back and forth along the barrier at velocity v_I. Another interesting feature of the mode spectrum, illustrated in Fig. 2, is the set of level crossings that occur at large values of $|g|$. The degeneracies occur when the ratio of $2P'/v_f$ to $2W/v_I$ is a rational number n/m with n and m being both odd

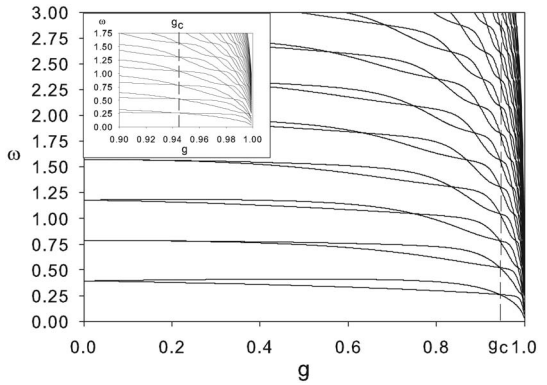

FIG. 2. The energy spectra calculated numerically are plotted from $g=0$ to 1. The spectrum is independent of the sign of g. For this illustration we choose $W=L=4$, $v_f=1$, which implies that $g_c \approx 0.943$. For $|g|<g_c$, mode splittings for each n are clearly seen, while for $|g|>g_c$, the spectrum bends toward low energy and evolves into two sets of equally spaced modes with distinct fundamental frequencies f_0 and f_I. The crosses mark the commensurability positions where $f_0/f_I=m/n$ with n, m both odd or both even.

or both even integers, and occur at frequencies $\omega_l = (n\pi v_f/P')l$, $l=1, 2,\ldots$.

Crossover Interaction Strength. $g^2=g_c^2=1-(W/P')^2$, the interaction strength for which $q_0P'=q_IW$ marks the crossover between weak and strong interaction limits. At $g=g_c$ the time required to travel at velocity v_I along the barrier is equal to the time required to travel a distance P' at velocity v_f along one of the chiral edge loops. In this case $f_0=f_I$ and the two strong interaction modes become degenerate. For $g>g_c$, the lowest-energy mode propagates primarily inside the interacting region, since the mode with lowest eigenfrequency is the mode with longest period T.

Quantum Edge Theory. The Hamiltonian in Eq. (1) can be solved quantum mechanically by bosonization. We define two sets of bosonic fields,

$$a_{L,k} \equiv \sqrt{\frac{2\pi}{kP}}\rho_L(-k), \quad a_{L,k}^\dagger \equiv \sqrt{\frac{2\pi}{kP}}\rho_L(k),$$

$$a_{R,k} \equiv \sqrt{\frac{2\pi}{kP}}\rho_R(k), \quad a_{R,k}^\dagger \equiv \sqrt{\frac{2\pi}{kP}}\rho_R(-k). \tag{9}$$

The Hamiltonian is readily expressed as a quadratic function of these bosonic fields. The normal mode solutions to the semiclassical equation of motion map to the independent oscillators of the quantum model in the usual way. The quantum version of the theory can be used to consider EM radiation absorption.

Power Absorption. Edge states couple to the EM fields via the Hamiltonian,[23]

$$H_{\text{ext}} = \frac{i}{\omega}\int_0^P dx(\vec{j}_L + \vec{j}_R)\cdot\vec{E}, \tag{10}$$

where $\vec{j}_L$, $\vec{j}_R$ are current operators for left and right QH samples, respectively, and the em waves of interest will typically have wavelengths much larger than the sample size. For simplicity we choose $W=L$ so that the geometry of the QH samples is square. The power absorption spectrum can be evaluated by Fermi's golden rule,

$$P(\omega) = 2\pi\sum_{\alpha,\beta}|\langle\alpha|H_{\text{ext}}|\beta\rangle|^2(E_\alpha - E_\beta)\delta(E_\alpha - E_\beta - \hbar\omega). \tag{11}$$

Peaks in the power absorption spectrum correspond to resonantly excited edge magnetoplasmons (EMPs).

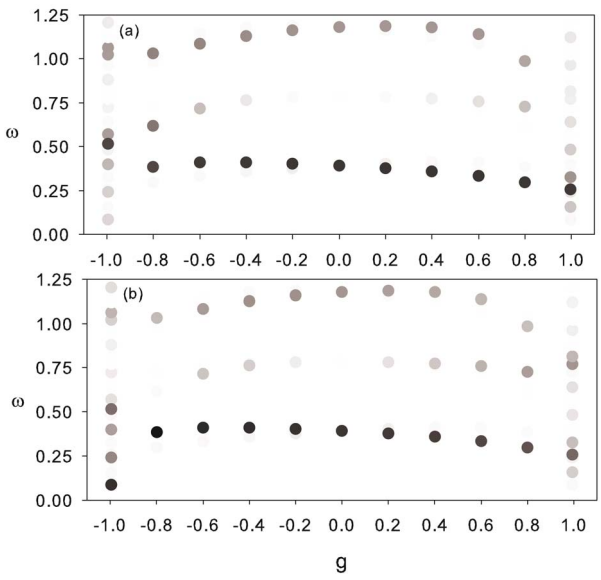

FIG. 3. (Color online) Resonant mode oscillator strength for $g=0$, $g=\pm0.2$, $g=\pm0.4$, $g=\pm0.6$, $g=\pm0.8$, and $g=\pm0.995$, with EM fields polarized (a) perpendicular to (b) along the narrow barrier. The strength of the each resonant absorption peak is indicated by the darkness of the circle.

Numerical results for the absorption spectrum are shown in Fig. 3. In general only the lowest few modes tend to have substantial absorption strength, because higher energy modes correspond to current oscillations with larger spatial varation leading to smaller matrix elements after integration along the edges. Although the energy spectrum does not depend on the sign of g, the mode absorption strengths at g and $-g$ does. For weak interactions the sharpest peak is for the lowest energy mode for repulsive interaction and at the *second* lowest energy mode for attractive interaction. This feature can be understood from the properties of the normal modes. For repulsive interactions the lowest-energy EMP has opposite charge densities on the left and right edges. Because currents flow in opposite directions in left and right edges, the net current is nonzero and coupling to the EM field does not vanish. For attractive interaction the energetic ordering of the two levels switches. The strongest absorption then occurs for the second lowest energy EMP.

The polarization of EM fields also influences the strength of peaks. It can be seen in Fig. 3 that for repulsive (attractive) interactions, the peak with EM fields orienated along the barrier line is weaker (stronger) than for polarization perpendicular to the barrier line. This occurs because the current

along the barrier is enhanced for attractive interactions and suppressed for repulsive interactions.

In the strong interaction limit, the localized EMPs modes propagate mainly in the barrier region and are not probed by EM fields polarized perpendicular to the barrier. As argued in previous sections, the current of those localized EMPs is small for repulsive interactions but not for attractive interactions. This property explains why EM fields applied along the barrier produce strong absorption at the lowest energy modes for $g=-0.995$ but not for $g=0.995$ in Fig. 3(b).

Comparison of Coulomb Model and Toy Model. A more realistic model can be obtained by replacing H_i in Eqs. (1) with both intra- and interedge Coulomb interactions. Since interactions on single isolated incompressible system edge to a good approximation influence only the mode velocity[17] and the interedge Coulomb interaction is much stronger in the barrier region than on other portions of the edge, we can expect the simple model properties to be similar to the realistic case. We have solved the more realistic Coulomb model numerically with the relative strength of interedge Coulomb interactions that can be tuned by changing the separation distance between left and right edges to verify this expectation. We conclude that the simple QHLJ model should be very useful for the interpretation of experimental results.

This work was supported by the Welch Foundation. The authors acknowledge helpful discussions with Matt Grayson, Woowon Kang, and Vittorio Pellegrini.

*Electronic address: leewc@mail.utexas.edu

†Electronic address: macd@physics.utexas.edu

[1] S. R. Renn and D. P. Arovas, Phys. Rev. B **51**, 16832 (1995).

[2] C. L. Kane and Matthew P. A. Fisher, Phys. Rev. B **56**, 15231 (1997).

[3] U. Zülicke and E. Shimshoni, Phys. Rev. Lett. **90**, 026802 (2003); Phys. Rev. B **69**, 085307 (2004).

[4] X. G. Wen, Phys. Rev. B **41**, 12838 (1990); Phys. Rev. Lett. **64** 2206 (1990); Phys. Rev. B **44**, 5708 (1991).

[5] B. I. Halperin, Phys. Rev. B **25**, 2185 (1982).

[6] A. H. MacDonald, Phys. Rev. Lett. **64** 220 (1990).

[7] C. W. J. Beenakker and M. Kindermann, Phys. Rev. Lett. **92**, 056801 (2004).

[8] W. Kang, H. L. Stormer, L. N. Pfeiffer, and K. W. West, Nature (London) **403**, 59 (2000); I. Yang, W. Kang, K. W. Baldwin, L. N. Pfeiffer, and K. W. West, Phys. Rev. Lett. **92**, 056802 (2004); I. Yang, W. Kang, L. N. Pfeiffer, K. W. Baldwin, K. W. West, E. A. Kim, and E. Fradkin, Phys. Rev. B **71**, 113312 (2005).

[9] M. Grayson, D. Schuh, M. Huber, N. Bichler, and G. Abstreiter, Appl. Phys. Lett. **86**, 032101 (2005); M. Grayson, D. Schuh, M. Bichler, M. Huber, G. Abstreiter, L. Hoeppel, J. Smet, and K. von Klitzing, Physica E (Amsterdam) **22**, 181 (2004).

[10] S. Roddaro, V. Pellegrini, F. Beltram, G. Biasiol, and L. Sorba, Phys. Rev. Lett. **93**, 046801 (2004); S. Roddaro, V. Pellegrini, F. Beltram, G. Biasiol, L. Sorba, R. Raimondi, and G. Vignale, Phys. Rev. Lett. **90**, 046805 (2003).

[11] R. de-Picciotto, M. Reznikov, M. Heiblum, V. Umansky, G. Bunin, and D. Mahalu, Nature (London) **389**, 162 (1997); Y. C. Chung, M. Heiblum, Y. Oreg, V. Umansky, and D. Mahalu, Phys. Rev. B **67**, 201104(R) (2003).

[12] L. Saminadayar, D. C. Glattli, Y. Jin, and B. Etienne, Phys. Rev. Lett. **79**, 2526 (1997).

[13] A. Mitra and S. M. Girvin, Phys. Rev. B **64**, 041309(R) (2001); A. Mitra and S. M. Girvin, *ibid.* **67**, 245311 (2003).

[14] M. Kollar and S. Sachdev, Phys. Rev. B **65**, 121304(R) (2002).

[15] E.-A. Kim and E. Fradkin, Phys. Rev. B **67**, 045317 (2003).

[16] E. Papa and A. H. MacDonald, Phys. Rev. Lett. **93**, 126801 (2004);E. Papa and A. H. MacDonald, Phys. Rev. B **72**, 045324 (2005).

[17] See, for example, U. Zulicke and A. H. MacDonald, Phys. Rev. B **54**, 16813 (1996).

[18] C. de C. Chamon and X.-G. Wen, Phys. Rev. B **49**, 8227 (1994); X. Wan, K. Yang, and E. H. Rezayi, Phys. Rev. Lett. **88**, 056802 (2002); K. Yang, *ibid.* **91**, 036802 (2003); M. D. Johnson and G. Vignale, Phys. Rev. B **67**, 205332 (2003).

[19] I. A. Larkin and V. B. Shikin, Phys. Lett. A **151**, 335 (1990); E. Papa and A. H. MacDonald (unpublished).

[20] M. Wassermeier *et al.*, Phys. Rev. B **41**, R10287 (1990); A. V. Polisskii *et al.*, J. Phys.: Condens. Matter **4**, 3955 (1992).

[21] I. Safi and H. J. Schulz, Phys. Rev. B **52**, R17040 (1995).

[22] R. D'Agosta, R. Raimondi, and G. Vignale, Phys. Rev. B **68**, 035314 (2003).

[23] G. D. Mahan, *Many-Particle Physics*, 3rd ed. (Kluwer Academic/Plenum Publishers, New York, 2000), Chap. 3.